CHEMCATCHEM

DOI: 10.1002/cctc.201000083

Temperature-Dependent Morphology, Magnetic and Optical Properties of Li-Doped MgO

Philipp Myrach,[a] Niklas Nilius,*[a] Sergey V. Levchenko,*[a] Anastasia Gonchar,[a] Thomas Risse,[a] Klaus-Peter Dinse,[b] Lynn A. Boatner,[c] Wiebke Frandsen,[a] Raimund Horn,[a] Hans-Joachim Freund,[a] Robert Schlögl,[a] and Matthias Scheffler[a]

Li-doped MgO is a potential catalyst for the oxidative coupling of methane, whereby surface Li^+O^- centers are suggested to be the chemically active species. To elucidate the role of Li in the MgO matrix, two model systems are prepared and their morphological, optical and magnetic properties as a function of Li doping are investigated. The first is an MgO film deposited on Mo(001) and doped with various amounts of Li, whereas the second is a powder sample fabricated by calcination of Li and Mg precursors in an oxygen atmosphere. Scanning tunneling and transmission electron microscopy are performed to characterize the morphology of both samples. At temperatures above 700 K, Li starts segregating towards the surface and forms irregular Li-rich oxide patches. Above 1050 K, Li desorbs from the MgO surface, leaving behind a characteristic defect pattern. Traces of Li also dissolve into the MgO, as concluded from a distinct optical signature that is absent in the pristine oxide. No electron paramagnetic resonance signal that would be compatible with Li^+O^- centers is detected in the two Li/MgO samples. Density-functional theory calculations are used to determine the thermodynamic stability of various Li-induced defects in the MgO. The calculations clarify the driving forces for Li segregation towards the MgO surface, but also rationalize the absence of Li^+O^- centers. From the combination of experimental and theoretical results, a detailed picture arises on the role of Li for the MgO properties, which can be used as a starting point to analyze the chemical behavior of the doped oxide in future.

Introduction

The transformation of abundant stable hydrocarbons into useful chemicals is a major task of today's basic research in catalysis.[1] In particular, methane activation has recently received considerable attention.[2,3] Oxidative coupling of methane (OCM) according to:

$$CH_4 + {}^1/_2\,O_2 \rightarrow {}^1/_2\,C_2H_4 + H_2O$$

with $\Delta_r H = -139\ kJ\,mol^{-1}$ at 800 °C has been a central focus of research. However, the underlying reaction mechanism is still not understood. For the reference catalyst, lithium-doped magnesium oxide, there is a heavily debated proposal for a mechanism that was put forward by Jack Lunsford several years ago.[4] The key step is hydrogen abstraction by O^- species, being created by Li doping and subsequent formation of Li^+O^- ion pairs. Lunsford et al. provided circumstantial evidence from a number of loosely connected experiments for a correlation between Li incorporation and the chemical activity of the doped oxide.[5,6] In a first class of experiments, $CH_3\cdot$ radicals were collected behind the Li/MgO catalyst bed by condensation of the OCM mixture on a cold finger, which was subsequently lowered into an EPR spectrometer to count the $CH_3\cdot$ radicals. In a second class of experiments, the Li/MgO material was annealed to 700 °C in air or pure O_2 instead of the OCM gas mixture and quenched afterwards at 77 K. After this treatment, the material was analyzed by EPR again. The signal at $g = 2.054$ was assigned to Li^+O^- centers, although no evidence for the spatial proximity of the paramagnetic defect and the Li^+ ion could be provided. From these, somewhat uncorrelated experiments, it was concluded that CH_4 molecules dissociate homolytically on the Li^+O^- centers into Li^+OH^- and $CH_3\cdot$ radicals. The latter would desorb into the gas phase where they would couple in a stoichiometric reaction, giving C_2H_6 as the primary C_2 product ($CH_3\cdot + CH_3\cdot \rightarrow C_2H_6$).

Given the lack of direct interconnection between the various pieces of evidence, we set out to systematically study the surface properties of Li-doped MgO, in order to revisit the proposed reaction mechanism. In this paper, we address mainly the structural and magnetic aspects of the problem. For this purpose, we carried out scanning tunneling microscopy (STM) and transmission electron microscopy (TEM) in combination

[a] P. Myrach, Dr. N. Nilius, Dr. S. V. Levchenko, A. Gonchar, Dr. T. Risse, W. Frandsen, Dr. R. Horn, Prof. Dr. H.-J. Freund, Prof. Dr. R. Schlögl, Prof. Dr. M. Scheffler
Fritz-Haber-Institut der MPG
Faradayweg 4-6,D-14195 Berlin (Germany)
Fax: (+49) 30-8413-4101
E-mail: nilius@fhi-berlin.mpg.de
sergey@fhi-berlin.mpg.de

[b] Dr. K.-P. Dinse
Fachbereich Physik, Freie Universität Berlin
Arnimallee,D-14195 Berlin (Germany)

[c] Dr. L. A. Boatner
Solid State Division, Oak Ridge National Laboratory
P.O. Box 2008, Oak Ridge, TN 37831

with optical and electron-paramagnetic resonance spectroscopy (EPR) on two model systems for Li-doped MgO. The first was a MgO thin film grown on Mo(001) with Li being incorporated during film preparation. The second was a Li/MgO powder catalyst that was fabricated by gel-combustion synthesis from $Mg(NO_3)_2/LiNO_3$/glycerol gels. In both cases, the Li induces a considerable roughening of the MgO surface at elevated temperatures due to segregation of dopants to the sample surface and defect formation. The thermodynamics of the underlying processes was revealed from ab inito calculations performed in addition. The surface modification of Li-doped MgO, with respect to the bare oxide, is considered an essential, yet disregarded precondition for the catalytic activity of the Li/MgO system.

Experimental and theoretical approach

Experiment

The experiments on thin MgO films were performed in an ultrahigh vacuum (UHV) STM operated at liquid-nitrogen temperature.[7] The STM was especially designed to detect photons from the tip–sample junction, and was able to probe optical properties with nanometer spatial resolution. For this purpose, a beetle-type STM head was surrounded with a parabolic mirror, which collects the emitted photons from a large solid angle and reflects them out of the UHV chamber towards a CCD-chip/grating-spectrograph unit. The photon emission is stimulated by electron injection from the tip into a well-characterized surface area and detected in a wavelength window between 200 to 1200 nm.

Pristine MgO films up to 15 monolayers (ML) in thickness were prepared by reactive Mg deposition in an O_2 ambience of 5×10^{-5} Pa onto a sputtered and flashed Mo(001) sample.[8] Subsequent annealing to 1100 K gave rise to a crystalline oxide film that completely wetted the Mo surface. The defect structure of the oxide was governed by an interfacial dislocation network with a periodicity of approximately 55 Å, being inserted into the film to compensate for the 5.4% lattice mismatch with the metal support.[9,10] In addition, a small number of domain boundaries, edge and screw dislocations were present in thicker films to release the remaining misfit strain. These line defects enclosed crystalline oxide patches that were several hundred nm^2 in size and slightly tilted with respect to the global surface plane (mosaics). This faceting of 10–15 ML thick films gave rise to distinct low-energy electron diffraction (LEED) reflexes, being characterized by four MgO[110]-oriented satellites around each primary reflex (Figure 1 a).[9] The satellites disappeared in films thicker than 20 ML due to a flattening of the oxide surface. Lithium was inserted into the oxide matrix by vapor deposition from a commercial SAES dispenser. Three preparation schemes were employed: a) Li deposition onto the surface of well-prepared MgO films; b) Mg–Li co-deposition onto Mo(001) in an O_2 atmosphere; c) sandwiching a Li–O plane between two thick MgO slabs. Details of the sample preparation, including the respective annealing procedures, are given later in the text.

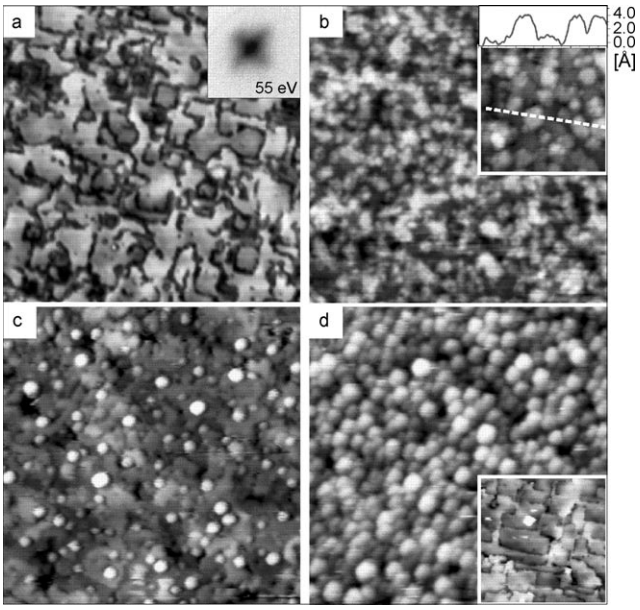

Figure 1. a) STM image of a 12 ML MgO/Mo film ($U_s=4.5$ V, 120×120 nm^2). The dark lines depict the network of dislocation lines that separate crystalline oxide patches; b) the same surface after deposition of approximately 1 ML Li at 300 K ($U_s=2.6$ V, 70×70 nm^2). The inset shows an enlarged surface area and a height profile along the dashed line (35×35 nm^2). The Li forms relatively flat islands on the MgO surface; c) the same preparation as in (b) but after annealing to 700 K for 10 min ($U_s=4.0$ V, 75×75 nm^2). Upon thermal treatment, the Li de-wets the MgO and forms hemispherical particles up to 15 Å in height; d) STM image of 12 ML MgO/Mo after deposition of 2 ML Li and annealing to 700 K ($U_s=4.0$ V, 75×75 nm^2). Again, a high density of Li-rich particles develops on the surface. The inset shows the same surface after annealing to 1050 K for 10 min. During heating, the surface Li desorbs and the pristine MgO film is recovered.

For the second part of the experiments, polycrystalline Li/MgO catalysts were prepared by a gel-combustion synthesis from $Mg(NO_3)_2/LiNO_3$/glycerol gels followed by calcination of the initially biphasic Li_2CO_3/MgO materials for 8 h at 1073 K in oxygen.[11] During this treatment, up to 97% of the originally present Li evaporated as LiOH, leaving the crystallites in a modified form with respect to the typical MgO nanocubes. The final crystallites had platelet shapes with rounded edges and typical diameters of about 50 nm. Due to their insulating nature, high-resolution imaging with SEM was impossible; however, the rough surface morphology of the crystallites was resolved by TEM using weak illumination and large primary beam diameters. EPR spectroscopy of MgO powders and Li-doped MgO single crystals was carried out on a Bruker ELEXYS E580 spectrometer using the Bruker Flexline X-Band ENDOR probe-head placed in a He cryostat. The Li-doped MgO films were investigated by continuous wave (cw) EPR spectroscopy under UHV conditions using a dedicated apparatus.[12]

Theory

To analyze the composition and defect structure of the Li/MgO(001) surface and morphological changes upon annealing, we applied an ab initio atomistic thermodynamic approach.[13]

The chemical potential of Li as a function of temperature and oxygen pressure is hereby determined for fixed Li concentrations in the MgO bulk. From this starting point, the formation and surface energies are expressed for the different compositions in order to simulate the experimental situation. The energies are calculated with periodic density functional theory (DFT) using the Perdew–Burke–Ernzerhof (PBE) generalized-gradient approximation to the exchange-correlation functional. Spin effects are fully taken into account by standard spin-density approaches. The slab model includes five layers of MgO with a 2×2 surface unit cell and 8 Mg and 8 O ions per layer. All surface structures considered here are generated from flat MgO(001) by introducing different elementary point defects and their combinations. The following defect types have been taken into account: a) Substitution of Mg by Li in the MgO lattice, referred to hereafter as Li_{Mg}; b) O, Mg, and Li adatoms; c) O and Mg vacancies, as well as O–Mg vacancy pairs; d) combinations of the defect types (b) and (c) with Li_{Mg}. The concentration of substitutional defects and vacancies ranges from 12.5 to 100 atom% for the respective species in a layer. Additional calculations for bulk MgO defects are preformed with a 64-atom $2\times2\times2$ unit cell. All geometries are fully relaxed. The defects are only introduced on one side of the slab surfaces, because such an approach provides the best balance between accuracy and computational cost. By analyzing the relaxation and formation energies, we demonstrated that the slab surfaces are well decoupled from each other. The calculations are performed with the electronic structure program FHI-aims using all-electron numerically tabulated atomic-orbital basis sets.[14] The basis sets are tested for convergence by ensuring that defect formation energies do not change by more than 0.02 eV. For the calculation of formation energies, we use the PBE total energy of an O_2 molecule corrected for the binding energy error: $E_{O_2}^{corr} = E_{O_2}^{PBE} + 0.56$ eV. This correction is based on the experimental value of 5.12 eV.[15] With this correction, the calculated formation enthalpies for Li_2O and MgO bulk oxides are close to the experimental values.

Results and discussion

Morphology of the Li/MgO films

Figure 1a shows an STM topographic image of an as-prepared MgO/Mo film 12 monolayers (ML) in thickness. The film consists of rectangular oxide patches delimited by dislocation lines. Due to the low conductivity of the oxide, the imaging was performed in the field-emission regime at bias voltage above 4.5 V. In this operation mode of the STM, the contrast is governed by work-function modulations on the surface.[16] The appearance of the dislocation lines as dark troughs therefore indicates their locally enhanced work function with respect to the defect-free oxide patches, an effect that can be explained by electron trapping in the line defects.[17,18]

After exposing the film to 1 ML Li at 300 K, the patched structure disappeared and the surface became covered with flat, 30–60 Å-wide islands (Figure 1b). The islands were, on average, two layers high (3.5–4 Å). Due to the high coverage, no obvious correlation between the dislocation network and the Li nucleation sites could be observed. Gentle annealing of the sample to 700 K induced a de-wetting of the MgO film, whereby the Li agglomerates into hemispherical particles 10–15 Å in height and up to 25 Å in diameter (Figure 1c). Those particles exclusively nucleated along the MgO dislocation lines, exposing the bare MgO patches in between. From the STM data, it cannot be ruled out that a fraction of the Li also penetrates the line defects. In fact, such an effect is suggested from the vanishing work-function contrast of the dislocation network, being induced by Li incorporation into the line defects. At higher Li exposure, both the size and density of the Li aggregates increased. In the STM image shown in Figure 1d, the MgO surface is almost completely covered with three-dimensional Li-rich particles that had formed after annealing to 700 K. Further annealing to 1050 K stimulated Li desorption from the surface, leaving behind the original, patched MgO film. However, we will demonstrate later that Li does not completely desorb and some material dissolves into the MgO film.

Two additional procedures were carried out to disperse the Li directly into the MgO matrix during growth. In the first, Li and Mg, with an atomic ratio of 1:5, were codeposited under an O_2 atmosphere onto the Mo support (referred to hereafter as mixed films). In the second approach, MgO and Li_xO layers were put down sequentially (termed sandwich films). Figure 2a displays an STM image of a mixed Li/MgO film that has been

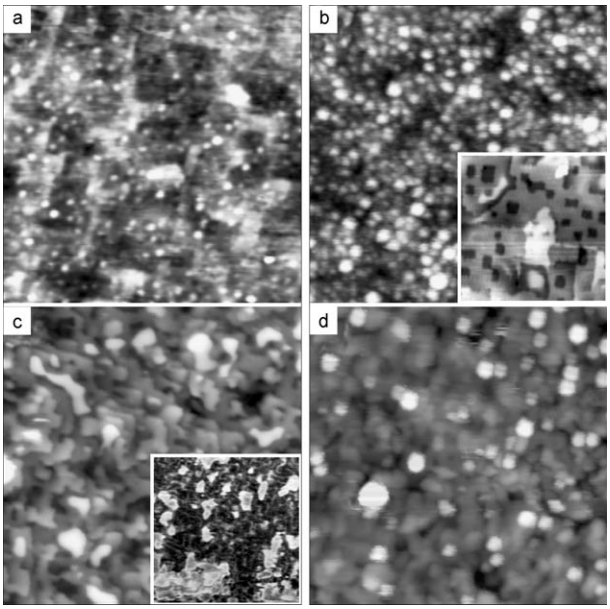

Figure 2. a) STM image of a 12 ML thick oxide film prepared by co-depositing Li and Mg in an O_2 ambience ($U_s = 5.0$ V, 100×100 nm^2). The Li/Mg atom ratio was set to 1:5; b) The same sample after annealing to 700 K (100×100 nm^2) and 1050 K (inset; 40×40 nm^2). Whereas at moderate temperatures, Li-containing clusters appear on the surface, they desorb at 1050 K and leave behind a pattern of rectangular holes; c) STM image of a sandwich film consisting of 5ML MgO–2ML Li_xO–5ML MgO annealed to 500 K ($U_s = 6.0$ V, 75×75 nm^2). The inset shows a conductance image taken at 6.8 V that reflects the variations in the electronic structure across the surface; d) STM image of a 5ML MgO–2ML Li_xO–5ML MgO sandwich film annealed to 700 K ($U_s = 6.0$ V, 75×75 nm^2).

annealed to 500 K in order to stimulate crystallization. Careful inspection of the topography still reveals the characteristic patch-structure of the pristine MgO film, albeit without the dark network of dislocation lines. In addition, small adparticles roughly 10 Å in height and 20 Å in diameter are present on the surface. The LEED pattern of the mixed films is indistinguishable from the original MgO LEED. Apparently, the MgO is able to incorporate a large portion of the Li into its rock-salt structure and only the surplus material either segregates to the surface or agglomerates within the MgO line defects. The latter effect is surmised from the disappearance of the work-function contrast of the dislocation network that would dominate the STM image otherwise. After annealing the sample to 700 K, large adparticles 15–20 Å in height and up to 60 Å in diameter emerged on the surface (Figure 2b). As the LEED pattern remains unchanged and only the background intensity rises, we suggest a phase separation has occurred between MgO in the film and disordered Li_xO aggregates on the surface. The morphology of the film changed once more upon annealing to 1050 K, when the adparticles desorbed and a macroscopically flat MgO surface developed (Figure 2b, inset). However, the new top layer is entirely covered with monolayer-deep rectangular holes, left behind by the desorbing Li_xO species. As mentioned before, even this high-temperature treatment was not able to remove all Li from the system, as demonstrated by optical spectroscopy (discussed later).

The last preparation explored in this study comprises a 5 ML MgO–2 ML Li_xO–5 ML MgO sandwich structure. After annealing to 500 K, the film exhibits a rough surface with a high density of small terraces (Figure 2c). Adjacent terraces often exhibit different electronic properties, as indicated by the pronounced contrast in differential conductance (d*I*/d*V*) STM images (Figure 2c, inset). The d*I*/d*V* signal provides a measure of the local density of states and the contrast therefore suggests a deviating electronic structure and hence a different chemical composition of neighboring oxide terraces.[16] A possible explanation for this observation might be a different Li/Mg ratio in the different surface regions. From a crystallographic point of view, the sandwich films are dominated by the rock-salt structure of MgO, as no additional reflexes are detected in LEED. In analogy to the mixed films, the sandwich structure decomposed at elevated temperature. Heating the film above 700 K led to the appearance of Li-containing clusters on the surface, whose density and size increased with temperature. Flashing the sample at 1050 K removed those aggregates from the surface, leaving behind a flat MgO film covered with rectangular holes. In general, the holes are less abundant and smaller than for the mixed oxide films, suggesting that less Li has reached the surface and evaporated into the gas phase.

The morphology of all three films prepared here conclusively indicates the presence of Li in the system. Whereas Li, in an unknown composition, is bound to the MgO surface after direct deposition, it only arrives at the surface of the doped films after annealing to temperatures above 700 K. In all cases, the Li induced a considerable surface roughening that was not fully reversed even after evaporating the Li compounds at around 1050 K. The latter observation is not unique for metal-supported Li/MgO films, but was also detected for Li/MgO powder samples produced by calcination at 1073 K. TEM images of individual oxide particles are shown in Figure 3. Figure 3a displays two crystallites with a platelet (left) and a more cubic shape (right). Along their edges, the typical stepped structure of normal MgO is seen as a sharp contour. The edge length is hereby of the order of 1 nm for higher indexed facets, but considerably longer for [100]-oriented steps. On the flat surface, a rectangular pattern of presumably atomic height is resolved. Figure 3b shows the rounded edge of a larger particle with the projection of a step structure being resolved to the left of the image. The rectangular pattern becomes visible on the flat parts of the crystallite. Tilting experiments demonstrated that this pattern is not a projection artifact of an edge structure, but occurs exclusively on flat (001)-oriented terraces. With increasing Li content, the particles grow into large platelets of micrometer size, exposing mainly (001) and irregular, high-indexed prismatic facets. However, the rectangular pattern remains visible on the basal planes of the crystallites with essentially unchanged dimensions. In general, this pattern is of similar appearance to the rectangular holes in well-annealed Li/MgO films observed with STM, suggesting the same origin of both structures. We will discuss the relation between this hole pattern and the Li dopants in a later section.

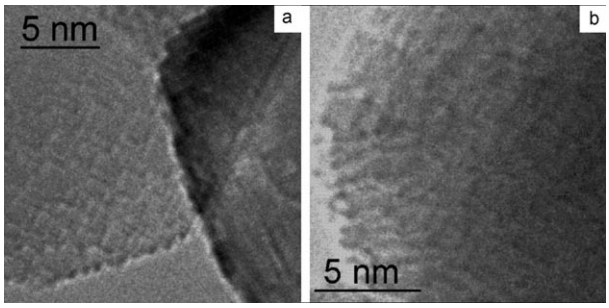

Figure 3. TEM images of Li-doped MgO nanoparticles prepared by gel combustion synthesis at 1073 K. The (001)-oriented facets are covered with a rectangular network that is similar to that observed on the doped films after high temperature treatment. See text for further discussion.

Optical properties of Li/MgO films

Classical optical spectroscopy on Li-doped MgO/Mo films was not feasible due to the small film thickness and the opaque nature of the metal support. We therefore employed fluorescence spectroscopy performed by injecting 100 eV electrons from the STM tip into the surface (accumulation time = 60 s per spectrum, electron current = 1 nA). This approach has the additional advantage that topographic and optical information can be acquired from the same surface area. It should be noted that prolonged electron bombardment gives rise to structural damage of the film that becomes manifest in the appearance of irregularly shaped holes. The surface modification

is ascribed to desorption of volatile species, such as oxygen or lithium.

The optical response of the bare MgO films of 12 ML thickness is dominated by an asymmetric emission peak centered at 410 nm (3.0 eV; Figure 4). A comparable optical signature

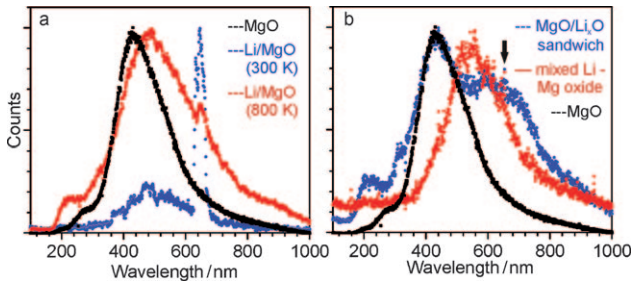

Figure 4. a) Photon-emission spectra of 12 ML MgO/Mo(001) (black), after deposition of 1 ML Li (blue) and after annealing to 800 K (red). The radiation was stimulated by the injection of 100 eV electrons at 1 nA current; b) Emission spectra of 12 ML MgO/Mo(001) (black), a layered MgO–Li_xO–MgO film annealed to 500 K (blue) and a Li-doped MgO film annealed to 700 K (red). The arrow indicates Li *D*-transitions. The spectral parameters are identical to those for (a).

was earlier observed in the photoluminescence spectra of MgO nanocubes and smokes[19,20] and assigned to the radiative decay of Frenkel excitons trapped at threefold coordinated lattice sites.[21] Corners and kinks, as the relevant traps of excitons in the oxide surface, are abundant in the MgO/Mo films as well, suggesting a similar emission mechanism in the present case.[10] The small shoulder at 300 nm (4.1 eV) relates to exciton recombination at fourfold coordinated lattice sites located at MgO step edges. This luminescence channel has also previously been identified on MgO nanocubes.[20] Exposing the MgO film to Li quenches the exciton-mediated light emission, most likely because the relevant surface sites are blocked by the adlayer and excitons decay nonradiatively. However, a new emission peak at 640 nm (1.93 eV) is detected for the Li-covered sample, which has a full-width-at-half-maximum (FWHM) of only 90 meV (Figure 4a). This peak is unusually narrow for an optical transition in a solid material, but compatible with emission processes in gas-phase species. Furthermore, it is well established that electron injection into alkali-containing systems (e.g. alkali halides) induces efficient desorption of the alkali species, which reach their ground state via radiative transitions in the gas-phase.[22,23] The 640 nm emission peak is therefore assigned to an optical de-excitation of Li species that have desorbed from the MgO film upon electron impact. The complete mechanism involves electron-mediated neutralization of Li ions, followed by their thermal desorption as the electrostatic attraction to the surface vanishes. The atoms are then post-excited by a second electron in a near-surface region and finally return to the ground state via photon emission.[22] The relevant optical transition of gas-phase Li is a decay of the $1s^2 2p^1$ excited state ($^3P_{3/2}$ and $^3P_{1/2}$ configuration) to the $1s^2$ $2s^1$ ground state ($^2S_{1/2}$), commonly known as the *D*-transition. In a field-free environment, the emitted photon has a wavelength of 670 nm,[24,25] which shifts to 640 nm due to the Stark effect introduced by the large electric field in the STM junction.[26] The narrow emission peak at 640 nm therefore provides a clear indication that Li is present at the MgO surface.

Annealing the Li/MgO adsystem to 800 K leads to substantial changes in the emission behavior (Figure 4a). First, the characteristic *D*-transition peak is strongly suppressed, suggesting a loss of Li from the surface. Secondly, the exciton-mediated MgO peak reappears, although with broader width and an intensity maximum shifted to longer wavelengths. The exact peak position varies between 480 and 560 nm (2.6 and 2.2 eV, respectively), depending on the initial Li coverage and the annealing temperature. This altered emission behavior reflects the opening of a new decay channel for the MgO excitons that involves Li-induced defect states in the MgO band gap. It is interesting to note that the MgO exciton band remains shifted even after complete removal of the surface Li at 1050 K (see inset of Figure 1d for the respective morphology), which indicates that a certain amount of Li dissolves into the MgO matrix and modifies its optical response. A detailed discussion of the emission mechanism in Li-doped MgO is beyond the scope of this work and will be presented in a forthcoming paper. At this point, the shifted MgO emission peak is taken as a fingerprint for the incorporation of Li into the MgO matrix.

Comparable emission behavior was revealed for the mixed Li/MgO films with an initial atom ratio of 1:5. Weakly annealed films exhibit a weak and broad emission band centered at 545 nm (2.25 eV), which becomes sharper and more intense after annealing to 700 K (Figure 4b). Further annealing reduces the emission intensity again; however the shifted line remains visible for temperatures as high as 1050 K. The Li *D*-transitions are also detected, indicating Li segregation towards the surface upon heating (arrow in Figure 4b). The emission behavior of the sandwich MgO–Li_xO–MgO film is also depicted in Figure 4b. After moderate tempering, the spectrum is characterized by low- and high-wavelength peaks at 410 nm (3.0 eV) and 590 nm (2.1 eV), respectively, being of similar width (FWHM = 750 meV). Whereas the low-wavelength peak matches the exciton band of the pristine MgO surface, the higher peak is ascribed to optical transitions in the Li_xO interface layer. This assignment is reasonable as the fundamental band gap of the most stable Li_2O compound is approximately 20% smaller than that of bulk MgO, rationalizing the down-shift of the respective exciton energies.[27] The two peaks of the sandwich film merge to a single one at 545 nm (2.3 eV) upon annealing to 700 K. Apparently, Li diffuses out of the interface layer into adjacent MgO patches and towards the surface at higher temperature. Upon prolonged thermal treatment, the optical response of the sandwich film gradually approached that of the mixed oxide layer, indicating substantial Li dispersion in the MgO matrix. Also the 640 nm peak appears again in the spectra of well-annealed films, demonstrating the presence of surface Li.

In summary, Lithium has two effects on the luminescence properties of doped MgO films. Whereas surface species produce a sharp emission band that reflects the radiative de-exci-

tation of desorbing Li atoms, dispersed Li in the oxide matrix opens a new decay channel for the MgO excitons. Preliminary optical studies on the polycrystalline Li/MgO samples reveal an increasing intensity of those absorption bands that are connected to three- and fourfold coordinated sites in the surface.[20] Apparently, the concentration of such sites increases with higher Li load, which is compatible with the Li-induced surface roughening of the crystallites discussed before. Details of the optical studies on Li/MgO powder samples are discussed elsewhere.[11]

EPR spectroscopy of the Li-doped MgO

From a mechanistic point of view, Li^+O^- centers are thought to play a crucial role for the chemical properties of the system. Due to their paramagnetic nature, EPR spectroscopy was used to verify their existence and elucidate their role in methane activation.[4,5] Consequently, we set out to investigate the systems discussed above by means of EPR spectroscopy to establish the presence of Li^+O^- centers.

The MgO powder samples were explored with the so-called field swept echo technique. The idea is to detect the echo intensity after a $\frac{\pi}{2}$–τ–π–τ–echo sequence as a function of the applied field. This produces an absorption spectrum, in contrast to conventional cw-EPR spectroscopy that gives 1 st derivative line shapes. The EPR spectra for the Li/MgO powders display no hint of the presence of paramagnetic Li^+O^- centers.[11] This result is in line with previous reports from the Lunsford group, in which paramagnetic Li^+O^- centers were only found upon heating Li/MgO powders in an oxidative environment and quenching them at low temperature.[6] To probe the general possibility of our setup to detect Li^+O^- centers, we also investigated Li-doped MgO single crystals, provided by L. A. Boatner from the Oak Ridge National Laboratories. Figure 5a shows an echo-detected EPR spectrum of an MgO single crystal containing a large concentration of transition metal impurities such as Fe and Mn. A high-resolution spectrum taken around the g_{zz} component at $g = 2.0549$ reveals a quartet of lines, as expected for an unpaired electron coupled to a Li nucleus with nuclear spin of $\frac{3}{2}$ (Figure 5a, inset). This quartet is identical to that previously described for Li-doped MgO single crystals.[28] To verify this assignment, we carried out an electron nuclear double-resonance (ENDOR) experiment (Figure 5b). The spectrum is characterized by a doublet of lines with a splitting of 6.88 MHz. The doublet is centered at 5.62 MHz, close to the nuclear Larmor frequency of Li at the applied magnetic field. The position of the signal in the EPR spectra in combination with the ENDOR data unambiguously proves the presence of Li^+O^- centers in the single crystals. Conversely, the absence of any signal in the powder samples allows us to conclude that the concentration of Li^+O^- centers is significantly lower than those of transition metal impurities, which were found in ppm concentrations. Besides the powder samples, we investigated the previously discussed Li-doped MgO films by means of EPR spectroscopy at ultrahigh vacuum (UHV) conditions. Irrespective of the preparation conditions, the samples gave rise to no evidence of paramagnetic Li^+O^- centers. However, it was shown that the setup is in principle able to detect sub-monolayer quantities of neutral Li adatoms[29] and O^- centers on the MgO(001) surface at 35 K.

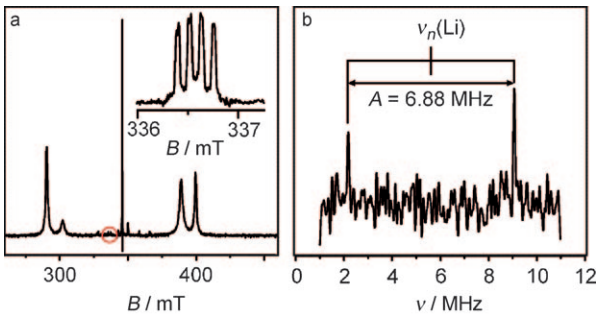

Figure 5. a) Echo-detected EPR spectrum of a Li-doped MgO single crystal taken at 10 K; pulse sequence: 40 ns ($\frac{\pi}{2}$ pulse), 500 ns, 80 ns (π pulses). The lines below 300 and above 350 mT are assigned to Fe and Mn impurities; inset: small field region of the g_{zz} component ($g = 2.054$) measured with high resolution at 5 K; pulse sequence: 160 ns ($\frac{\pi}{2}$ pulse), 1200 ns, 320 ns (π pulses). The splitting between the quartet of lines corresponds to a hyperfine coupling constant of 6.8 MHz; b) Davis ENDOR spectrum (stochastic mode, $T = 5$ K) of the same sample taken at 336.79 mT; pulse sequence (MW channel): 240 ns (π pulse), 22000 ns, 120 ns ($\frac{\pi}{2}$ pulses), 500 ns, 240 ns (π pulses).

Morphological and thermodynamic aspects

Li deposition onto MgO/Mo films at 300 K, the first system investigated here, gave rise to the formation of large, flat Li islands on the oxide surface. This finding is compatible with an earlier calorimetry/DFT study of Li adsorption on MgO.[30,31] It was demonstrated therein that Li nucleation is defect-mediated and governed by structural inhomogeneities in the oxide surface. The calculated Li binding energy ranged from 3.4 eV at MgO kink sites to 1.6 eV at step edges, in good agreement with the measured heat of adsorption at low exposure of 2.6 eV.[30] In contrast, binding to oxygen vacancies on the flat surface turned out to be unfavorable (0.55 and 1.3 eV for F^0 and F^+ centers) and occurs only for kinetic reasons. Beyond the nucleation regime, Li atoms attach to the existing aggregates in a highly exothermic process, which explains the development of surface clusters. Kinetically, the formation of 2D islands is preferred due to a relatively large barrier for up-step diffusion, while thickening of the aggregates mainly proceeds via Li atoms that directly land on pre-existing islands. It was therefore concluded that Li wets the MgO surface at room temperature, as confirmed by our STM data (Figure 1b). Furthermore, the structural inhomogeneities that initiate Li nucleation are now identified as the line defects in the MgO film. Only close to the thermodynamic equilibrium, that is, on well-annealed samples, formation of 3D particles is expected, as the calculated attachment energy for Li is only 10% larger for 3D than for 2D particles.[29,30] The deduced de-wetting behavior at elevated temperature is clearly visible in our STM images taken after sample annealing (Figure 1c, d).

To assess the thermodynamic stability and electronic properties of Li dissolved in the MgO matrix, new DFT calculations were carried out with the theoretical approach described

before. The formation energy of substitutional Li atoms at Mg sites (Li_{Mg} defects), as calculated with the PBE functional, is lowest for the MgO(001) top layer and monotonically increases for deeper layers. Already in the third layer, the Li_{Mg} formation energy is virtually identical to the MgO bulk value, indicating a fast convergence of the Li properties when going away from the surface. However, the overall changes in energy are small (ca. 0.1 eV) and within the error bar of the method. DFT with standard functionals in general is not the best choice for describing the Li_{Mg} defects as it underestimates the hole localization. However, the layer-dependent Li_{Mg} formation energy is known to be insensitive to the degree of localization.[32] The Li_{Mg} formation energy also depends on the initial Li concentration in the respective layer. In the top layer, the stabilization is largest if 50% of the Mg atoms are replaced by Li ($Li_{50}Mg_{50}$ islands, Figure 6). In deeper layers, this coverage dependence is less pronounced and no stable Li–Mg compositions are revealed.

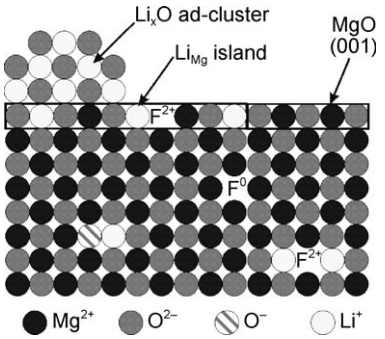

Figure 6. Surface and bulk structures related to Li-doping of MgO(001). See text for details.

The Li_{Mg} defects strongly interact with O vacancies in the film.[33] In fact, the formation energies for O vacancies in the MgO (001) surface are significantly reduced in the presence of nearby Li (Figure 7). Analysis of the electronic structure reveals the origin of the Li_{Mg}-mediated destabilization of lattice oxygen. The monovalent Li^+ that replaces a divalent Mg^{2+} exerts a lower Coulomb attraction on the O^{2-}. It also provides acceptor states near the MgO valence band that can be filled by an electron transfer out of the vacancy (*p*-type doping). Vacancy formation is therefore highly favorable from a thermodynamic point of view, in particular if the initial F^0-center transfers its electrons to the unsaturated oxygen ions next to the Li_{Mg} defects. In fact, the resulting F^{2+}-center in the vicinity of a pair of Li_{Mg} defects has a 6 eV lower energy than an isolated F^0-center plus two uncompensated Li_{Mg} defects in the surface (Figure 7). We have also calculated the temperature-dependent concentrations of various defect types in Li-doped MgO, using the experimental O_2 pressure of 5×10^{-5} Pa. At low temperature, the concentration of Li_{Mg} and O adatoms adsorbed from the gas phase is very high. However, this situation is thermodynamically unfavorable and gives rise to the spontaneous formation of surface Li_xO (Figure 6). As the temperature rises, the equilibrium concentration of O adatoms decreases rapidly and Li_{Mg} defects accompanied by O vacancies segregate to the surface. This scenario is in good agreement with the experimental situation, in which the development of Li-containing surface clusters was observed at elevated temperature (Figure 2b, d).

So far we have not taken into account any interaction between the Li_{Mg} defects. This interaction could lead to the formation of Li_{Mg} surface islands, because the interaction for Li_{Mg} in the top layer is attractive at 0 K. However, Li_{Mg} aggregation at finite temperature is only expected if the loss in configurational entropy due to island formation is compensated by the reduction in total energy. To address this point, we estimated the surface formation energy for two limiting cases: a) atomically dispersed Li_{Mg} defects in the top layer of MgO(001), and b) islands containing 50% Li_{Mg} defects and 50% Mg atoms. Formation of $Li_{50}Mg_{50}$ islands in the top layer is indeed favorable in a broad temperature window. Only above a critical temperature do the islands start to shrink, as the Li dissolves into the bulk due to entropy or desorbs into the gas phase. Not surprisingly, this critical temperature is lower if the bulk concentration of Li_{Mg} defects is smaller. To complete the picture, we have determined the concentration of O adatoms and vacancies within the $Li_{50}Mg_{50}$ islands. The resulting phase diagram for the top layer is shown in Figure 8. At 300 K and

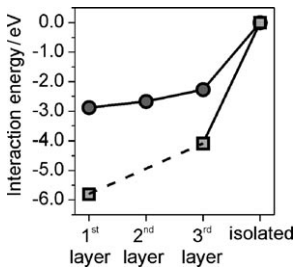

Figure 7. Interaction energy between Li_{Mg} defects in different layers and an O vacancy in the top layer of MgO (001). The stabilization of the defects is stronger when the Li_{Mg}/vacancy ratio is two (squares) and the vacancies become F^{2+}-centers, than for a Li_{Mg}-defect ratio of one(circles), whereupon F^+-centers are formed.

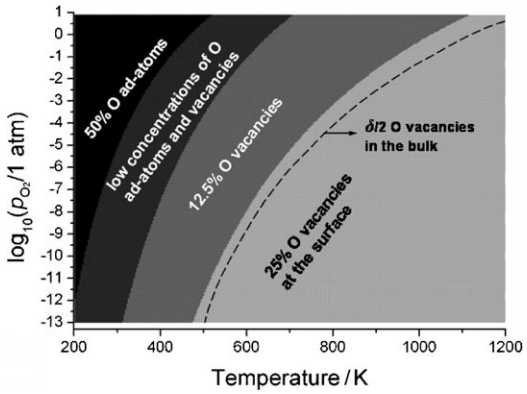

Figure 8. Phase diagram of the MgO(001) surface with 50% Li_{Mg} in the top layer ($Li_{50}Mg_{50}$ islands). The dashed curve marks the situation at which the thermodynamically favored concentration of O vacancies, given by 50% of the Li_{Mg} concentration, is reached in the bulk. 1 atm = 101 325 Pa.

experimental pressure conditions, the amount of O adatoms and vacancies is negligible. As the temperature increases, a high concentration of O vacancies builds up in the $Li_{50}Mg_{50}$ islands until the energetically preferred situation of 25% vacancies is reached (corresponding to one F^{2+}-center stabilizing two Li_{Mg} defects). Also the bulk concentration of O vacancies increases towards the final value of 50% of the Li_{Mg} bulk concentration. This situation corresponds again to the case that a pair of Li_{Mg} defects interacts with a single F^{2+} center. The (T, p) curve at which the saturation density of O vacancies is reached in the MgO bulk is depicted by the dashed line in the phase diagram shown in Figure 8.

Based on these theoretical results, we suggest the following interpretation of the experimental data: The morphological evolution of mixed Li/MgO films with temperature is dominated by Li segregation towards the surface, followed by the formation of Li_{Mg} surface islands with 50% substitutional Li ions. The presence of even more Li gives rise to the formation of Li_xO surface clusters (Figures 1 and 2). This process is very efficient due to the high initial concentration of Li_{Mg} in the film of approximately 15% and is responsible for the observed surface roughening. Upon annealing, the Li_xO evaporates first, exposing the MgO(001) surface with the embedded $Li_{50}Mg_{50}$ islands. Those islands continue to lose Li and O and finally desorb at 1050 K, leaving behind the characteristic pattern of rectangular holes in the MgO surface. The situation is similar for the MgO-Li_xO-MgO sandwich films, only that the final Li_{Mg} concentration at the surface is smaller as a part of the Li is fixed directly at the interface in the form of Li_xO. Also here, Li_{Mg} segregation sets in at intermediate temperatures (ca. 500 K) and leads to the formation of $Li_{50}Mg_{50}$ islands. Although these islands cannot be identified in STM topographies, their different electronic structure with respect to bare MgO gives rise to the contrast observed in the dI/dV maps (Figure 2c, inset). Only at temperatures above 700 K has enough Li_{Mg} accumulated at the surface to produce Li_xO adclusters. Flashing the sample to 1050 K triggers again the desorption of Li_{Mg} and surrounding O ions, producing the characteristic hole pattern in the films.

The fact that the same defect pattern is observed in TEM images of Li/MgO crystallites indicates that the sequence of Li segregation, formation of Li-rich islands, and evaporation at high temperature described for thin films occurs in a similar way for the powder samples (Figure 3). This compatibility underlines the possibility of exploring Li-doped MgO with surface science techniques on simplified systems such as crystalline oxide films grown on metal supports. The absence of the expected EPR signal for Li^+O^- centers can also be explained with the DFT results. Due to their large formation energy, such centers are thermodynamically highly unfavorable with respect to paired Li_{Mg} defects plus a single F^{2+} vacancy. Both defect types do not host unpaired electrons and are therefore EPR silent.[34] It needs to be emphasized however that our results do not exclude the general possibility to form Li^+O^- centers, especially at conditions far away from the thermodynamic equilibrium.[5]

Conclusion and Outlook

Different preparation techniques have been combined to produce Li-doped MgO films and powder samples as model systems to explore the catalytic performance of this material in the oxidative coupling of methane. In this work, we have mainly concentrated on the physical properties of the doped oxide, in particular on the impact of Li on the morphological, optical and magnetic properties of the MgO host. At low concentration and temperature, the Li incorporates into the MgO matrix most likely in combination with oxygen vacancies. Those Li-induced defects give rise to a distinct change in the optical response of the system. Annealing above 500 K triggers the segregation of substitutional Li towards the surface, where it first accumulates in mixed Li-Mg oxide islands and later forms phase-separated Li_xO clusters. The segregation is accompanied by a considerable surface roughening, as observed by the different microscopic techniques. At temperatures above 1050 K, the Li desorbs from the surface, leaving behind a characteristic pattern of rectangular holes. However, even prolonged heating is insufficient to completely remove the Li from the MgO matrix, as demonstrated by a deviating optical response with respect to pristine MgO. The formation of Li^+O^- centers, which are commonly connected to the catalytic activity of the doped oxide, could not be approved by EPR spectroscopy, either in thin-film or in powder samples. This finding is consistent with the results of DFT calculations that indicated the thermodynamic instability of such centers in a large pressure and temperature window. However, the development of Li^+O^- centers might still be possible at non-equilibrium conditions that have not been explored in our study. A number of topics, for instance the effect of Li on the electronic and optical properties of MgO, could only be briefly discussed in this work and will be the subject of a forthcoming study. However, our results provide a reliable starting point to reexamine the reaction mechanism proposed for the oxidative methane coupling on Li/MgO catalysts.

Acknowledgements

The authors thank U. Zavyalova for preparing the Li/MgO powder samples. S. V. L. acknowledges support by the Alexander von Humboldt foundation. This work has been partially funded by the DFG through the 'Cluster of Excellence UNICAT.'

Keywords: doping · EPR spectroscopy · lithium · optical analysis · scanning probe microscopy

[1] G. Ertl, *Angew. Chem.* **2008**, *120*, 3578; *Angew. Chem. Int. Ed.* **2008**, *47*, 3524.
[2] E. Morales, J. H. Lunsford, *J. Catal.* **1989**, *118*, 255.
[3] T. Ito, J. H. Lunsford, *Nature* **1985**, *314*, 721.
[4] J. H. Lunsford, *Angew. Chem.* **1995**, *107*, 1059; *Angew. Chem. Int. Ed. Engl.* **1995**, *34*, 970.
[5] D. J. Driscoll, W. Martir, J. X. Wang, J. H. Lunsford, *J. Am. Chem. Soc.* **1985**, *107*, 58.
[6] J. X. Wang, J. H. Lunsford, *J. Phys. Chem.* **1986**, *90*, 5883; T. Ito, J. X. Wang, C. H. Lin, J. H. Lunsford, *J. Am. Chem. Soc.* **1985**, *107*, 5062.

[7] N. Nilius, A. Cörper, G. Bozdech, N. Ernst, and H.-J. Freund, *Prog. Surf. Sci.* **2001**, *67*, 99.
[8] Y. D. Kim, J. Stultz, D. W. Goodman, *Surf. Sci.* **2002**, *506*, 228.
[9] S. Benedetti, H. M. Benia, N. Nilius, S. Valeri, H.-J. Freund, *Chem. Phys. Lett.* **2006**, *430*, 330.
[10] S. Benedetti, P. Torelli, S. Valeri, H. M. Benia, N. Nilius, G. Renaud, *Phys. Rev. B* **2008**, *78*, 195411.
[11] R. Zavyalova, I. Oprea, S. Mavlyankariev, F. Girgsdies, T. Risse, H. J. Freund, K. P. Dinse, R. Schlögl, **2010**, unpublished results.
[12] J. Schmidt, T. Risse, H. Hamann, H.-J. Freund, *J. Chem. Phys.* **2002**, *116*, 10861.
[13] a) K. Reuter, M. Scheffler, *Phys. Rev. B* **2001**, *65*, 035406; b) C. M. Weinert, M. Scheffler, *Mater. Sci. Forum* **1986**, *10–12*, 25; c) M. Scheffler, J. Dabrowski, *Philos. Mag. A* **1988**, *58*, 107.
[14] V. Blum, R. Gehrke, F. Hanke, P. Havu, V. Havu, Xinguo Ren, K. Reuter, M. Scheffler, *Comp. Phys. Comm.* **2009**, *180*, 2175.
[15] K. P. Huber, G. Herzberg, *Molecular Spectra and Molecular Structure. IV. Constants of Diatomic Molecules*, Van Nostrand Reinhold Co., New York, **1979**.
[16] N. Nilius, *Surf. Sci. Rep.* **2009**, *64*, 595 – 659.
[17] H. M. Benia, P. Myrach, N. Nilius, *New J. Phys.* **2008**, *10*, 013010.
[18] K. P. McKenna, A. L. Shluger, *Nat. Mater.* **2008**, *7*, 859.
[19] M. Anpo, Y. Yamada, Y. Kubokawa, S. Coluccia, A. Zecchina, M. Che, *J. Chem. Soc. Faraday Trans. 1* **1988**, *184*, 751.
[20] S. Stankic, M. Müller, O. Diwald, M. Sterrer, E. Knözinger, J. Bernardi, *Angew. Chem.* **2005**, *117*, 4996; *Angew. Chem. Int. Ed.* **2005**, *44*, 4917.
[21] A. L. Shluger, P. V. Sushko, L. N. Kantorovich, *Phys. Rev. B* **1999**, *59*, 2417.
[22] a) *Desorption Induced by Electronic Transitions: DIET II* (Eds.: W. Brenig, D. Menzel), Springer, Berlin, **1985**; b) *Desorption Induced by Electronic Transitions: DIET III* (Eds.: R. H. Stulen, M. L. Knotek), Springer, Berlin, **1988**.
[23] M. Wilde, I. Beauport, F. Stuhl, K. Al-Shamery, H. J. Freund, *Phys. Rev. B* **1999**, *59*, 13401.
[24] W. A. van Wijngaarden, G. A. Noble, *Lect. Notes Phys.* **2008**, *745*, 111.
[25] G. A. Noble, B. E. Schultz, H. Ming, W. A. van Wijngaarden, *Phys. Rev. A* **2006**, *74*, 012502.
[26] R. Ashby, J. J. Clarke, W. A. van Wijngaarden, *Eur. Phys. J. D* **2003**, *23*, 327.
[27] L. Liu, V. E. Henrich, *Phys. Rev. B* **1996**, *54*, 2236.
[28] M. M. Abraham, Y. Chen, L. A. Boatner, R. W. Reynolds, *Phys. Rev. Lett.* **1976**, *37*, 849.
[29] J. C. Lian, E. Finazzi, C. Di Valentin, T. Risse, H. J. Gao, G. Pacchioni, H. J. Freund, *Chem. Phys. Lett.* **2008**, *450*, 308.
[30] J. A. Farmer, C. T. Campbell, L. Xu, G. Henkelman, *J. Am. Chem. Soc.* **2009**, *131*, 3098.
[31] J. A. Farmer, N. Ruzycki, J. F. Zhu, C. T. Campbell, *Phys. Rev. B* **2009**, *80*, 035418.
[32] M. Nolan, G. W. Watson, *Surf. Sci.* **2005**, *586*, 25.
[33] Z. Yang, G. Liu, R. Wu, *Phys. Rev. B* **2002**, *65*, 235432.
[34] Another reason for the absence of Li^+O^- centers in thin MgO films might be electron tunneling from the Mo(001) support into the hole centers.

Received: March 20, 2010
Published online on June 22, 2010

